

Article

Optimizing the Salt-Processing Parameters of *Achyranthes bidentata* and Their Correlation with Anti-Osteoarthritis Effect

Jieqiang Zhu ¹, Lisha Shen ¹, Guofang Shen ² and Yi Tao ^{1,*} 

¹ College of Pharmaceutical Science, Zhejiang University of Technology, Hangzhou 310014, China; zhujieqiang@zjut.edu.cn (J.Z.); 221122070262@zjut.edu.cn (L.S.)

² Hangzhou Food and Drug Inspection and Research Institute, Hangzhou 310022, China; shengf@126.com

* Correspondence: taoyi1985@zjut.edu.cn

Abstract: *Achyranthes bidentata* is always salt-processed before being prescribed for treating osteoarthritis. Yet the salt-processing parameters have not been optimized, and the specific bioactive constituents responsible for the osteoarthritis effect of salt-processed *A. bidentata* have not been fully elucidated. In this study, a Box–Behnken experimental design was chosen for the optimization of the salt-processing parameters of *A. bidentata*, including stir-frying time, concentration of brine, and soak time. Meanwhile, HPLC–Q-TOF-MS was utilized to analyze the chemical profiles of various batches of raw and salt-processed *A. bidentata*. The anti-inflammatory potential of nine batches of both raw and salt-processed *A. bidentata* was assessed via a cyclooxygenase-2 (COX-2) inhibitory assay. A gray correlation analysis was conducted to correlate the peak areas of the compounds in raw and salt-processed *A. bidentata* with their COX-2 inhibitory effects. Finally, the optimal salt-processing conditions are as follows: soak time: 29 min; concentration of brine: 1.8%; stir-frying time: 4.4 min. Twenty-nine compounds were identified. Eight compounds were found to have a strong positive correlation with anti-inflammatory activity, as confirmed by the COX-2 inhibitory assay. Notably, this is the first report of the COX-2 inhibitory effects of sanleng acid, stachysterone D, dihydroactinidolide, *N*-cis-feruloyl-3-methoxytyramine, 9,12,13-trihydroxy-10-octadecenoic acid, azelaic acid, and dehydroecdysone.

Keywords: *Achyranthes bidentata*; salt-processing; cyclooxygenase-2; anti-inflammatory



Citation: Zhu, J.; Shen, L.; Shen, G.; Tao, Y. Optimizing the Salt-Processing Parameters of *Achyranthes bidentata* and Their Correlation with Anti-Osteoarthritis Effect. *Processes* **2024**, *12*, 434. <https://doi.org/10.3390/pr12030434>

Academic Editor: Ibrahim M. Abu-Reidah

Received: 24 January 2024
Revised: 12 February 2024
Accepted: 18 February 2024
Published: 21 February 2024



Copyright: © 2024 by the authors. Licensee MDPI, Basel, Switzerland. This article is an open access article distributed under the terms and conditions of the Creative Commons Attribution (CC BY) license (<https://creativecommons.org/licenses/by/4.0/>).

1. Introduction

Traditional methods for processing crude herbs distinctly differentiate traditional Chinese medicine from Western medicine. These methods encompass sauteing with rice wine [1,2] or brine, steaming with water or rice wine [3], frying with sand [4,5] or oil, and braising with rice wine or licorice liquids. The primary objective of processing is to eliminate or diminish toxicity and side effects, alter nature and actions, and enhance therapeutic effects. Simultaneously, to guarantee safety and efficacy, it is essential to rigorously control and regulate the quality of processed products.

Achyranthes bidentata, as one of the “four major Huai medicines,” is mainly cultivated in Henan province. The chemical constituents of *A. bidentata* include oleanolic acid glycosides, saponins, ecdysterone, ketosteroids, and flavonoids [6]. Although modern pharmacological studies have shown that *A. bidentata* has a plethora of bio-activities, including anti-osteoarthritis [7], improving memory [8], regulating blood sugar level [9], preventing apoptosis [10], promoting angiogenesis, UV protection [11], anti-convulsion [12], anti-osteoporosis [13], improving xerophthalmia [14], and alleviating acute kidney injury [15], this herb is commonly used in the clinical treatment of osteoarthritis. After being salt-processed, the effects will be dramatically enhanced. However, the salt-processing parameters for *Achyranthes bidentata* have not been optimized yet.

Quality by design (QbD) is a concept in the pharmaceutical and biopharmaceutical industries endorsed by regulatory agencies such as the U.S. Food and Drug Administration

(FDA) [16]. The key principles of QbD involve the systematic identification of critical product attributes and process parameters and understanding how these factors influence product quality. Experimental design methods were always used. The salt-processing method for *Achyranthes bidentata* includes several process parameters, such as stir-frying time, concentration of brine, and soak time. How these process parameters affect the quality of salt-processed *Achyranthes bidentata* needs to be understood.

Salt-processed *Achyranthes bidentata* is prescribed for treating osteoarthritis. The anti-inflammatory effect is the critical product attribute of salt-processed *Achyranthes bidentata*. Cyclooxygenase-2 (COX-2), also known as prostaglandin oxidase synthase (PTGS-2), is a bifunctional enzyme with both cyclooxygenase and catalase activities. COX-2 inhibitors have played a significant anti-inflammatory role in vivo and in vitro [17]. *A. bidentata* can reduce the expression of COX-2 in the synovial tissue of joints through the arachidonic acid pathway and exert therapeutic effects on osteoarthritis [7]. The results suggested that the anti-osteoarthritis effect of *A. bidentata* is associated with COX-2; however, the compounds of *A. bidentata* that are attributed to the anti-inflammatory effects are poorly understood.

The aim of this work is to optimize the salt-processing parameters of *A. bidentata* by using a Box–Behnken experimental design, apply HPLC–Q-TOF-MS analysis in conjunction with orthogonal partial least squares discriminant analysis to identify the differential markers between raw and salt-processed *A. bidentata*, and obtain the quality markers for the anti-inflammatory activity of salt-processed *A. bidentata* by using COX-2 inhibition assay and gray correlation analysis.

2. Materials and Methods

2.1. Instruments and Chemicals

Agilent 1290 high-performance liquid chromatography (Agilent Technology Co., Santa Clara, CA, USA); PD-1D-50 freeze dryer (Beijing Boyikang Experimental Instrument Co., Beijing, China); UPLC-Triple TOF 5600+ high-resolution mass spectrometry system (Waters Corporation/AB Sciex Corporation, Framingham, MA, USA); Tecan sunrise multifunctional microplate reader (Diken Trading Co., Shanghai, China).

Acetonitrile was obtained from Tedia Company, Inc. (Fairfield, OH, USA); Methanol from Sinopharm Chemical Reagent Co., Shanghai, China; *n*-butanol from Sinopharm Chemical Reagent Co.; PBS buffer from Shanghai Yuanye Biotechnology Co., Shanghai, China; COX-2 inhibitor screening kit from Biyuntian Biotechnology Co., Shanghai, China; Nine batches of *A. bidentata* were collected from Wen County, Henan Province, and authenticated by Professor Wang Ping of Zhejiang University of Technology. Voucher specimens were deposited in the herbarium of the College of Pharmaceutical Science, Moganshan campus of Zhejiang University of Technology. Standard substances with purities > 98%, including ecdysterone, 25R-inokosterone, and 25S-inokosterone, were obtained from the China Institute for Food and Drug Control; Sanleng acid, 9,12,13-trihydroxy-10-octadecenoic acid, and azelaic acid were obtained from Chengdu Must Biological Technology Co., Chengdu, China (purities > 98%); Dihydroactinidiolide, *N*-cis-feruloyl-3-methoxytyramine, *N*-trans-feruloyltyramine, dehydroecdysone, and stachysterone D were obtained from Sichuan Weikeyi Biological Technology Co., Chengdu, China (purities > 98%). Maleic acid and fumaric acid were obtained from Sinopharm Chemical Reagent Co., Shanghai, China (purities > 98%).

2.2. Optimization of Salt-Processing Procedure for *A. bidentata*

Dried roots of *A. bidentata* were immersed in brine for a period. After that, the roots were transferred to the wok with gentle heat and stir-fried for a while. Finally, the salt-processed *A. bidentata* was allowed to cool.

Three parameters, including soak time, concentration of brine, and stir-frying time, were investigated in the present study to optimize the processing conditions. The software Design Expert (Trial Version 7.0.3, Stat-Ease Inc., Minneapolis, MN, USA) was employed for experimental design, data analysis, and model building. Box–Behnken designs with three

variables were used to determine the response pattern and then to establish a model. Three variables with three levels of each variable were used for the optimization of magnetic solid-phase extraction: soak time (X1), concentration of brine (X2), and stir-frying time (X3). The 2020 edition of Chinese Pharmacopeia takes ecdysterone as a quality indicator of *Achyranthes bidentata*. In the optimization of processing conditions, the dependent variable (Y) was the concentration of ecdysterone.

2.3. HPLC–Q-TOF-MS Analysis

The conditions for HPLC chromatography were as follows: The chromatographic column was Agilent Kromasil C₁₈ (4.6 mm × 250 mm, 5.0 μm). The injection volume was set to 20 μL. The mobile phase consisted of acetonitrile (A) and 0.1% formic acid water (B). The gradient elution program was as below: 0 min–3 min, 16–20% A; 3 min–10 min, 20–23% A; 10 min–20 min, 23–26% A; 20 min–35 min, 26–40% A; 35 min–45 min, 40–50% A; 45 min–50 min, 50–60% A; 50 min–51 min, 60% to 15% A; 51 min–60 min, 15% A. The flow rate was set to 1 mL·min⁻¹. The column temperature was adjusted to 40 °C. The detection wavelength was 250 nm.

The samples were analyzed with Waters Synapt G2 Q-TOF (Milford, MA, USA) mass spectrometry, which was equipped with an electron spray ionization (ESI) source. The internal calibration for mass accuracy is sodium formate. The first step is an initial correction with sodium formate. After passing the test, the standard curve will be made. After passing the test, the real-time internal standard correction will be made. The MS conditions were as follows: the mass acquisition was performed under negative ionization mode; the scanning range was 100 Da to 1000 Da; the scanning time was 0.2 s; the capillary voltage was 3000 V; the cone voltage was 30 V; the ion source temperature was 120 °C; the desolvent-free flow rate was 800 L·h⁻¹; and the desolvation temperature was 350 °C. The mass data were analyzed using Masslynxtv 4.2 software.

2.4. COX-2 Inhibitory Assay

The inhibitory assay of COX-2 was measured according to the method previously described with slight modifications [18]. A total of 75 μL aliquot of COX-2 buffer was added to a 96-well plate, and then 5 μL of COX-2 cofactor solution, 5 μL of COX-2 solution, and 5 μL of test solution of *A. bidentata* sample or single compound were added subsequently. The 96-well plate was incubated at 37 °C for 10 min. Then, a 5 μL aliquot of the COX-2 fluorescence probe was added. After that, a 5 μL aliquot of COX-2 substrate solution was added and mixed at 37 °C for 5 min constantly. The 96-well plate was put into the microplate reader. The excitation wavelength was set to 560 nm, and the emission wavelength was set to 590 nm. Celecoxib was selected as the positive control. A total of 5.0 mL of aqueous extract of raw and salt-processed *A. bidentata* was added to 5.0 mL phosphate-balanced saline (pH = 7.4) and thoroughly mixed. The mixture was centrifuged, and the supernatant was sent for a COX-2 inhibitory assay. A gradient concentration of standard substance solutions including sanleng acid, stachysterone D, dihydroactinidiolide, *N*-*cis*-feruloyl-3-methoxytyramine, *N*-*trans*-feruloyltyramine, 9,12,13-trihydroxy-10-octadecenoic acid, azelaic acid, and dehydroecdysone were prepared with phosphate-balanced saline (pH = 7.4). The inhibition rate of the sample solutions was calculated.

2.5. Gray Correlation Analysis

The peak area of each compound in nine batches of raw and salt-processed *A. bidentata* and the COX-2 inhibition rate were input into the gray modeling software (Version 7) to conduct the correlation analysis. The correlation coefficient *r* between each compound and COX-2 inhibitory activity was obtained. The correlation coefficient *r* > 0.85 can be considered a very strong positive correlation [19].

2.6. Chemometric Analysis

The peak area of each compound in the nine batches of raw and salt-processed *A. bidentata* was subjected to the software SIMCA-P (version 13) for pattern recognition. An unsupervised pattern recognition method, i.e., principal component analysis, was first used for modeling. After that, a supervised method, i.e., orthogonal partial least squares discriminant analysis, was used to identify the differential compounds between raw and salt-processed *A. bidentata*. Variable importance plots of PLS-DA models were used to find significantly altered compounds (VIP value ≥ 1.0) [20].

3. Results and Discussion

3.1. Optimization of the Salt-Processing Procedure for *A. bidentata*

The Box–Behnken response surface method is a multifactor nonlinear experimental optimization method. This method is continuous over a range of experimental conditions and can be analyzed for any of these test-point conditions. Therefore, the Box–Behnken response surface method was chosen to optimize the salt-processing procedure [21]. The experimental framework for the Box–Behnken design (BBD) of salt-processing parameters, encoded numerically, included 17 randomized permutations. The optimization of the salt-processing protocol was gauged by the concentration of ecdysterone as the dependent variable. The specific experimental configurations and their outcomes are enumerated in Table 1.

Table 1. Box–Behnken design for optimization of the salt-processing procedure of *A. bidentata*.

Run	Independent Variable			Conc. of Ecdysterone ($\mu\text{g/mL}$)
	X1 (Soak Time, min)	X2 (Concentration of Brine, %)	X3 (Stir-Frying Time, min)	
1	30	2	5	485.571
2	30	1	7	305.3
3	10	2	7	395.933
4	30	3	7	395.356
5	50	2	7	391.509
6	50	3	5	389.812
7	30	2	5	488.776
8	10	3	5	421.638
9	30	2	5	484.89
10	10	2	3	410.132
11	30	2	5	486.46
12	30	1	3	446.888
13	10	1	5	436.884
14	50	2	3	457.694
15	30	2	5	480.762
16	50	1	5	438.679
17	30	3	3	463.877

An Analysis of Variance (ANOVA) was utilized to evaluate the statistical significance and adequacy of the model, with findings delineated in Table 2. Significance testing of each factor was conducted using F-tests and *p*-values. The model's F-value of 3.89 suggests statistical significance. Factors with *p*-values below the 0.05 threshold were considered significant. The ANOVA results indicated that the linear term for stir-frying time, as well as the quadratic terms for brine concentration and stir-frying time, had a significant impact on the concentration of ecdysterone.

Table 2. Estimated regression coefficients for the quadratic polynomial model.

Factor	Regression Coefficients	Standard Error	DF	F Value	Prob > F
B ₀	485.29	13.60	1	3.89	0.0435
Linear					
B ₁	1.64	10.75	1	0.0232	0.8831
B ₂	5.37	10.75	1	0.2493	0.6329
B ₃	−36.31	10.75	1	11.41	0.0118
Interaction					
β ₁₂	−8.41	15.20	1	0.3058	0.5975
β ₁₃	−13.0	15.20	1	0.7311	0.4208
β ₂₃	18.27	15.20	1	1.44	0.2685
Quadratic					
β ₁₁	−26.29	14.81	1	3.15	0.1193
β ₂₂	−37.25	14.81	1	6.32	0.0401
β ₃₃	−45.19	14.81	1	9.30	0.0186
Lack of fit			3	250.38	<0.0001
Pure error			4		
R ²	0.8334		Adjusted R ²	0.6192	

As is shown in Table 2, the value of the determination coefficient R^2 of 0.8334 indicated a good agreement between the observed and predicted values by the model. Response surface plots were employed for the visualization of the effect of two factors on the response. The interacting effect of soak time and concentration of brine is displayed in Figure 1A. A higher concentration of ecdysterone should be expected in the middle of the soak time, ranging from 10 to 50 min. This is because the brine regulates the osmotic pressure of the plant cells, which affects the texture of the hyssop after cooking. The interaction of stir-frying time with soak time is demonstrated in Figure 1B. The investigated system seems to perform better at the middle value of stir-frying time, ranging from 3 min to 7 min. High temperatures may destroy the chemical constituents. The effect of stir-frying time in relation to the concentration of brine is shown in Figure 1C. With the increase in brine concentration from 1% to 2.6%, the concentration of ecdysterone remains unchanged. The selected values of salt-processing conditions are presented in Table 3.

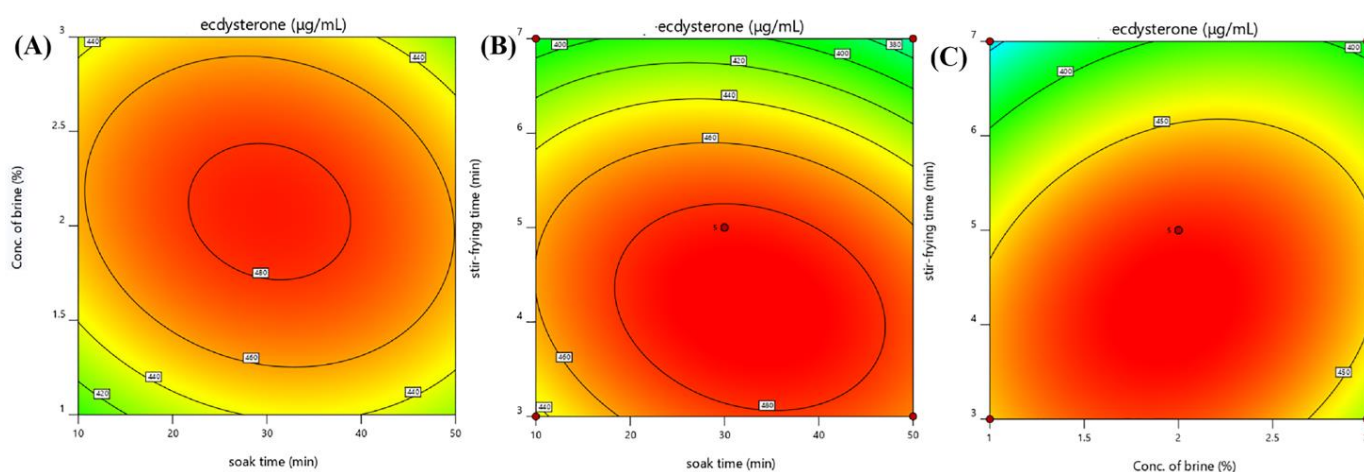


Figure 1. Response surface plots of the three factors. (A) interaction between concentration of brine and soak time; (B) interaction between stir-frying time and soak time; (C) interaction between stir-frying time and concentration of brine.

Table 3. Predicted and experimental response values under optimal conditions.

Factor	Value
Soak time (min)	29
Concentration of brine (%)	1.8
Stir-frying time (min)	4.4
Predicted values ($\mu\text{g}/\text{mL}$)	490.1
Experimental values ($\mu\text{g}/\text{mL}$)	491.79 ± 0.83

The real and predicted mean concentrations of ecdysterone under repeatability conditions are shown in Table 3. The experimental values of the concentration of ecdysterone were calculated at $491.79 \mu\text{g}/\text{mL}$. No significant difference ($p < 0.05$) was observed between the theoretical and experimental responses. The optimal conditions are as follows: soak time: 29 min; concentration of brine: 1.8%; stir-frying time: 4.4 min.

3.2. Characterization of Chemical Constituents of Raw and Salt-Processed *A. bidentata*

The HPLC–Q-TOF-MS method was employed to analyze the chemical compounds of raw and salt-processed materials under negative ion mode, and the total ion chromatograms (TIC) are shown in Figure 2. Twenty-nine compounds were identified by comparing them with standard compounds and related works of literature. The identification of chemical compounds and the variation ratio of the compounds in *Achyranthes bidentata* after and before salt processing are displayed in Table 4. Of note, the peak area ratios of compounds 2, 4, 7, 12, 13, and 22 were all above 10 after salt processing. Their structures are shown in Figure S1.

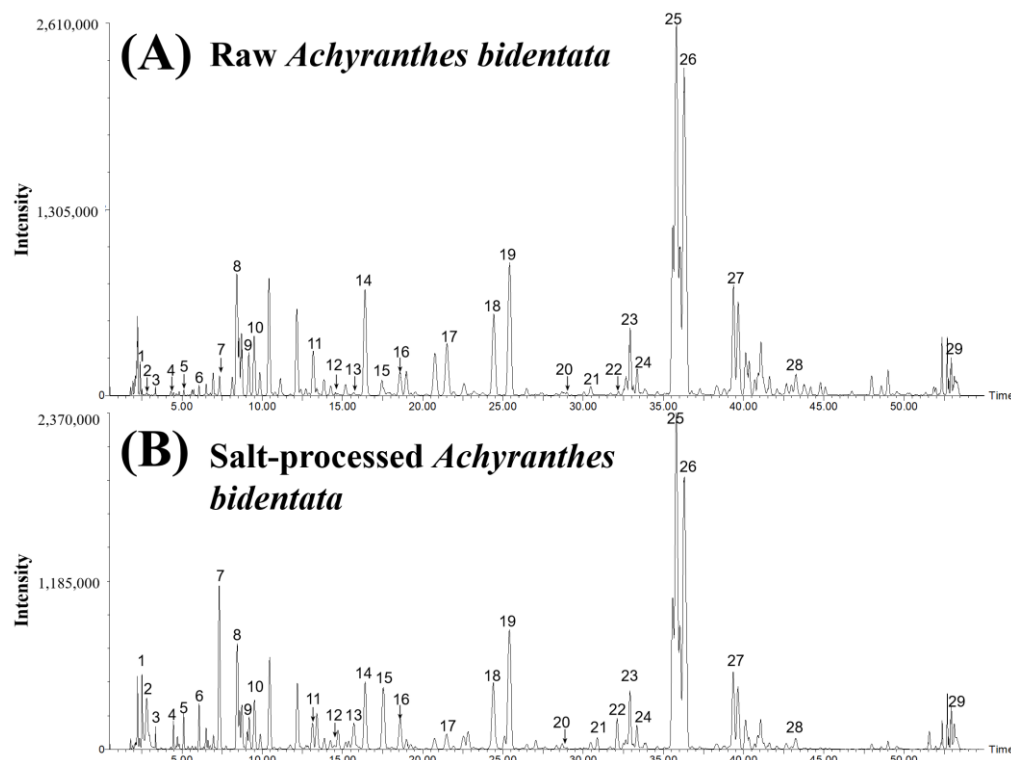


Figure 2. HPLC–Q-TOF-MS total ion chromatograms of raw and salt-processed *Achyranthes bidentata*. (A) raw *Achyranthes bidentata*; (B) salt-processed *Achyranthes bidentata*.

Table 4. Identification of chemical compounds in *Achyranthes bidentata*.

No.	t _R (min)	Detected Mass (m/z)	MS ²	Molecular Formula	Mass Error (ppm)	Compound (Name)	Identification	Peak Area Ratio
1	2.50	115.0036	100.0234, 99.0085, 99.9332	C ₄ H ₄ O ₄	4.3	Maleic acid	standards	1.91
2	2.81	115.0032	111.1115, 104.7421, 87.0104, 77.8366, 73.9177	C ₄ H ₄ O ₄	0.9	Unknown	—	26.59
3	3.34	115.0037	111.0400, 108.0446, 105.0223, 97.0370, 89.0271, 87.0083, 59.0153	C ₄ H ₄ O ₄	5.2	Fumaric acid	standards	2.04
4	4.47	204.0664	186.0639, 159.0353, 131.0420, 108.0486, 69.8676	C ₁₁ H ₁₁ NO ₃	1.5	Indolylactic acid	[22]	12.55
5	5.1	235.0757	220.0741, 187.0871, 141.6590, 122.0250, 94.0303, 93.0204, 77.4244	C ₁₆ H ₁₂ O ₂	−0.9	Methylflavone	[23]	6.97
6	6.07	541.3029	495.2991, 477.2920, 299.1640, 249.1525, 129.0598, 99.0488	C ₂₇ H ₄₄ O ₈	3.0	Polypodine B	[24]	4.93
7	7.32	210.0773	177.0686, 154.0703, 124.0408, 122.0292, 94.0312, 93.0255, 66.0354	C ₁₀ H ₁₃ NO ₄	3.3	Methoxytyrosine	[25]	10.63
8	8.43	525.3055	479.3034, 319.1958, 301.1819, 210.0828, 159.1058	C ₂₇ H ₄₄ O ₇	−1.7	Ecdysterone	standards	0.80
9	9.18	525.3040	479.3073, 443.1053, 377.1133, 346.1055, 319.1931, 301.1936, 282.1422, 261.1450, 217.1015, 186.0648, 159.1079, 141.0920, 124.0425	C ₂₇ H ₄₄ O ₇	−4.6	25R-inokosterone	standards	0.90
10	9.51	525.3048	479.3033, 477.2902, 159.1055	C ₂₇ H ₄₄ O ₇	−3.0	25S-inokosterone	standards	0.80

Table 4. Cont.

No.	t _R (min)	Detected Mass (m/z)	MS ²	Molecular Formula	Mass Error (ppm)	Compound (Name)	Identification	Peak Area Ratio
11	13.4	507.297	461.2921, 301.1889, 277.1472, 249.1255, 201.1278, 159.1051	C ₂₇ H ₄₂ O ₆	2.4	Dehydroecdysone	standards	7.28
12	14.7	507.296	461.2861, 345.1842, 309.1479, 265.1693, 229.0488, 159.1066, 115.0768, 83.0535	C ₂₇ H ₄₂ O ₆	1.0	Deoxykaladasterone	[26]	19.43
13	15.7	523.3109	477.3076, 459.2956, 361.2192, 317.1931, 159.1105	C ₂₇ H ₄₂ O ₇	−1.5	Kaladasterone	[27]	15.25
14	16.4	507.2959	461.2989, 403.2529, 301.1815, 249.1308, 209.1000, 159.1058, 83.0489	C ₂₇ H ₄₂ O ₆	0.2	Dacryhainansterone	[26]	0.58
15	17.5	187.0974	159.1022, 141.1016, 139.0442, 111.0111	C ₉ H ₁₆ O ₄	2.1	Azelaic acid	standards	4.38
16	18.6	549.1589	341.1035, 311.0556, 295.0618, 268.0379, 255.0433, 252.0448	C ₂₆ H ₃₀ O ₁₃	−4.4	Liquiritin apioside	standards	1.38
17	21.5	342.1357	327.1139, 190.0521, 178.0531, 148.0552, 135.0417, 134.0422	C ₁₉ H ₂₁ NO ₅	4.7	<i>N-cis</i> -feruloyl-3-methoxytyramine	standards	0.26
18	24.4	312.1246	190.0584, 178.0544, 148.0556, 135.0491	C ₁₈ H ₁₉ NO ₄	3.2	<i>N-trans</i> -feruloyltyramine	standards	0.81
19	25.4	342.1343	327.1171, 190.0533, 178.0529, 148.0544, 135.0460	C ₁₉ H ₂₁ NO ₅	1.2	Feruloyl-methoxytyramine	[28]	0.91

Table 4. Cont.

No.	t _R (min)	Detected Mass (m/z)	MS ²	Molecular Formula	Mass Error (ppm)	Compound (Name)	Identification	Peak Area Ratio
20	29.0	509.2856	494.1100, 489.6156, 466.2194, 421.8323, 410.1779, 387.1925, 384.8494, 358.5213, 350.2032, 342.0960, 333.4114	C ₃₂ H ₄₆ O ₅	−1.8	Unknown	—	2.26
21	30.5	225.1124	214.0546, 209.0778, 196.8297, 187.0986, 171.8831, 158, 1576, 144.2472, 130.0387, 116.0739, 98.9125, 96.5702	C ₁₁ H ₁₆ O ₂	−1.3	Dihydroac- tinidiolide	standards	0.65
22	32.1	507.2973	461.2921, 368.0941, 342.1358, 312.1195, 268.0684, 242.0818, 221.7878, 171.0949, 139.1091, 86.8855, 56.2580	C ₂₇ H ₄₂ O ₆	4.9	Stachysterone D	standards	10.49
23	32.9	327.2175	229.1391, 221.1249, 211.1358, 171.1032, 85.0286	C ₁₈ H ₃₂ O ₅	1.2	Corchorifatty acid F	[29]	0.87
24	33.4	327.2186	323.1074, 242.4109, 235.1030, 211.1431, 171.1025, 146.9710, 137.1052, 97.0710, 85.0290	C ₁₈ H ₃₂ O ₅	4.6	9,12,13- Trihydroxy- 10,15- octadecadienoic acid	[30]	0.93
25	35.8	329.2340	229.1482, 211.1358, 171.1053, 139.1160	C ₁₈ H ₃₄ O ₅	3.6	9,12,13- Trihydroxy- 10- octadecenoic acid	standards	0.51
26	36.3	329.2337	171.1043, 139.1148, 127.1147	C ₁₈ H ₃₄ O ₅	2.7	9,10,13- TriHOME	[31]	0.61

Table 4. Cont.

No.	t _R (min)	Detected Mass (m/z)	MS ²	Molecular Formula	Mass Error (ppm)	Compound (Name)	Identification	Peak Area Ratio
27	39.3	329.2334	211.2371, 199.1361, 197.1192, 181.1294, 169.1259, 129.0907, 99.0819	C ₁₈ H ₃₄ O ₅	1.8	Pinellic acid	[32]	0.71
28	43.2	329.2336	303.0145, 255.2305, 204.8009, 211.1199, 201.1148, 199.1152, 171.1017, 152.9974, 146.9705, 96.9641, 80.8853	C ₁₈ H ₃₄ O ₅	2.4	Sanleng acid	standards	0.55
29	53.2	643.3685	610.5566, 588.5043, 569.3351, 531.3790, 512.9322	C ₃₆ H ₅₄ O ₁₀	7.1	Unknown	—	0.80

Compounds **1**, **2**, and **3** showed the same [M–H]–ion at m/z 115, which corresponded to the formula of C₄H₄O₄. In comparison with standard compounds, compounds **1** and **3** were ambiguously identified as maleic acid and fumaric acid. Compound **4** at the retention time of 4.47 min displayed [M–H]–ion at m/z 204. Fragment ion at m/z 186 in the MS² spectrum was produced by losing one molecule of water. In comparison with the reference [22], compound **4** was unambiguously deduced as indolylactic acid. Compound **5** showed the [M–H]–ion at m/z 235 and produced an ion at m/z 220 with the loss of the methyl group. By comparing with a related reference [23], compound **5** was deduced as methylflavone. Compound **6** at the retention time of 6.07 min showed [M + HCOO]–ion at m/z 541. Fragment ions at m/z 495 were produced by losing one molecule of HCOOH in the MS² spectrum. Compound **6** was deduced as polypodine B by comparing it with the fragmentation pathway in the literature [24]. The precursor ion of compound **7** at m/z 210 produced a fragment ion at m/z 177, which was attributed to the loss of both the H₂O and CH₃ groups. In comparison with the reference [25], compound **7** was assigned as methoxytyrosine. With the retention times of 8.43 min, 9.18 min, and 9.53 min, compounds **8**, **9**, and **10** displayed the same [M + HCOO]–ion at m/z 525, as well as the characteristic neutral loss of 46 Da yielding the product ion at m/z 479, which was ascribed to the loss of the HCOOH group. Compared with the standard substances, compounds **8**, **9**, and **10** were unambiguously deduced as ecdysterone, 25*R*-inokosterone, and 25*S*-inokosterone, respectively [33]. In the same way, compounds **11**, **12**, **14**, and **22** shared the same [M + HCOO]–ion at m/z 507. The fragmentation of compounds **11**, **12**, **14**, and **22** produced an ion at m/z 461 with a neutral loss of HCOOH in the MS² spectrum. Compared with the reference [26], compounds **11**, **12**, **14**, and **22** were tentatively deduced as dehydroecdysone, deoxykaladasterone, dacryhainansterone, and stachysterone D, respectively. The molecular formula of compound **13** is 16 Da more than that of compound **12**, whereas the retention time of compound **13** is a little later than that of compound **12**. Compared with the literature, compound **13** was plausibly assigned as kaladasterone [27]. Compound **15** showed the [M–H]–ion at m/z 187, which corresponded to the formula of C₉H₁₆O₄. Compound **15** was deduced to be azelaic acid by comparing it with the mass information in the literature [34]. Compound **16** showed the parent ion at m/z 547 and

the daughter ion at m/z 255. Compared with the standard substance, compound **16** was unambiguously deduced as liquiritin apioside [35]. Compounds **17** and **19** shared the same $[M-H]^-$ ion at m/z 342 and yielded fragment ions at m/z 327, m/z 190, m/z 178, m/z 148, and m/z 135. The retention time of compound **19** was a little later than that of compound **17**. Compared with the standard substances, compounds **17** and **19** were unambiguously deduced as *N-cis*-feruloyl-3-methoxytyramine and feruloylmethoxytyramine [28]. Compound **18** showed the $[M-H]^-$ ion at m/z 312 and produced fragment ions at m/z 190, m/z 178, m/z 148, and m/z 135, which was consistent with the fragmentation pathway of *N-trans*-feruloyltyramine [36]. Compound **21** showed $[M-H]^-$ ion at m/z 225 with a formula of $C_{11}H_{16}O_2$. Compared with the literature [37], compound **21** was tentatively deduced as dihydroactinidiolide. Moreover, compounds **23** and **24** both shared the same $[M-H]^-$ ions at m/z 327, which corresponded to a formula of $C_{18}H_{32}O_5$. Compared with the references, compounds **23** and **24** were tentatively assigned as corchorifatty acid F [29] and 9,12,13-trihydroxy-10,15-octadecadienoic acid [30], respectively. Compounds **25**, **26**, **27**, and **28** were tentatively deduced as 9, 12, 13-trihydroxy-10-octadecenoic acid, 9,10,13-triHOME [31], pinellic acid [32], and sanleng acid [38], respectively.

3.3. Chemometric Analysis

Principal component analysis was first employed for the analysis of the data of the peak areas of 29 common peaks of nine batches of raw (S1, S2, S3, S4, S5, S6, S7, S8, S9) and salt-processed *A. bidentata* (Y1, Y2, Y3, Y4, Y5, Y6, Y7, Y8, Y9). The score and loading plots of the PCA model are displayed in Figure 3.

The samples of raw and salt-processed *A. bidentata* were well separated. Then, the supervised orthogonal partial least squares discriminant analysis method was used. The score and loading plots of the OPLS-DA model are shown in Figure 4. Q^2 of the OPLS-DA model is 97.6%, which indicates good prediction capability.

The score plot showed that the batches of raw *A. bidentata* were distinctly separated from the salt-processed batches. The VIP plot is sorted from high to low and shows confidence intervals for the VIP values, normally at the 95% level. VIP values larger than 1 indicate “important” X-variables, and values lower than 0.5 indicate “unimportant” X-variables. The importance projection of variables ($VIP > 1$) was used as the criteria to screen out the compounds that caused the difference. As depicted in Figure 5, methylflavone, indolylactic acid, maleic acid, methoxytyrosine, ecdysterone, 5-deoxy kaladasterone, pinellic acid, kaladasterone, fumaric acid, dactryhainansterone, polypodine B, 9, 12, 13-trihydroxy-10, 15-octadecadienoic acid, 25*R*-inokosterone, liquiritin apioside, and *N-trans*-feruloyltyramine were identified as compounds with VIP values greater than 1. The VIP (Variable Importance for the Projection) plot summarizes the importance of the variables both to explain X and to correlate to Y. These compounds were considered important X-variables.

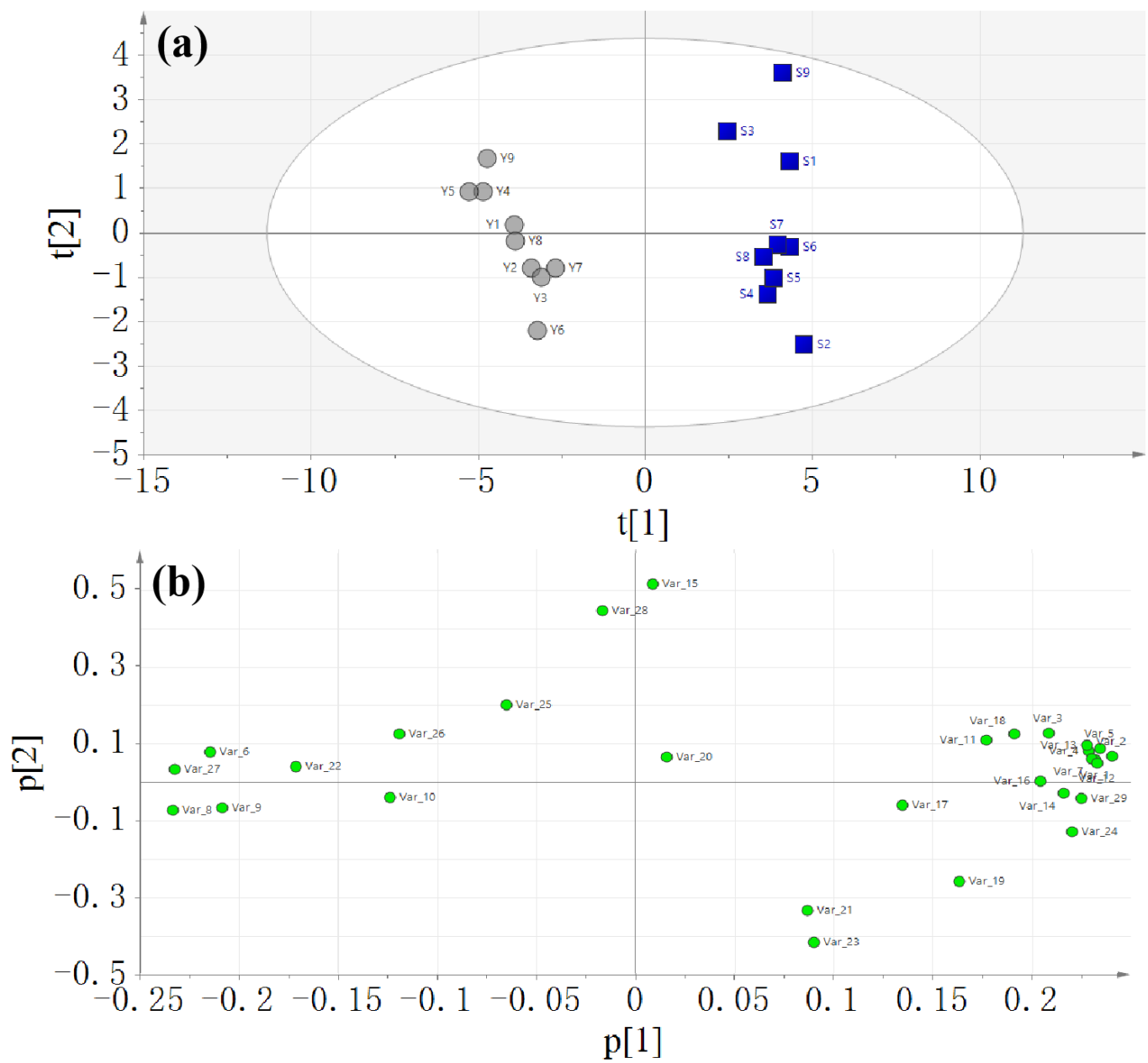


Figure 3. Score plot (a) and loading plot (b) of the principal component analysis.

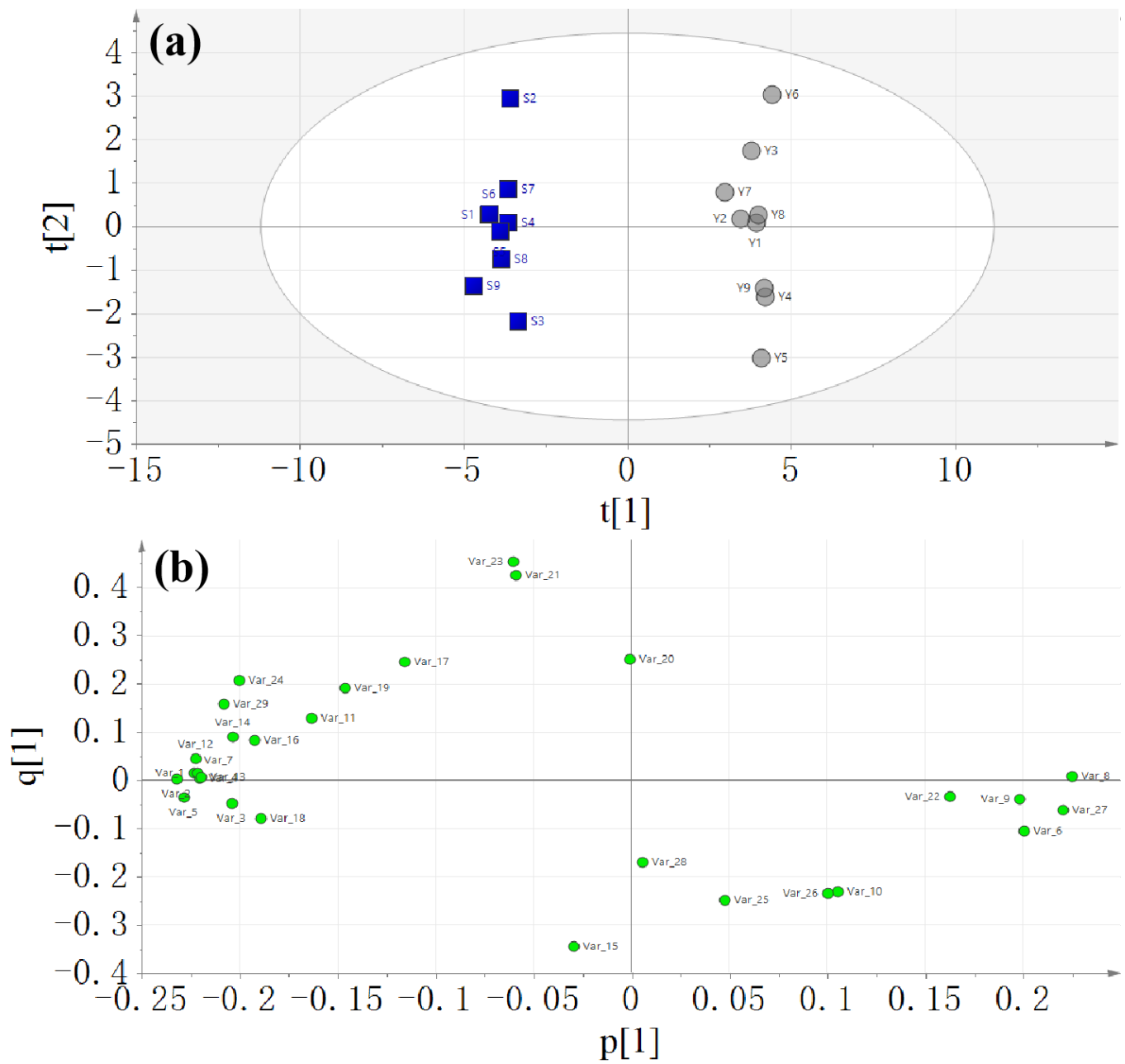


Figure 4. Score plot (a) and loading plot (b) of the OPLS-DA model.

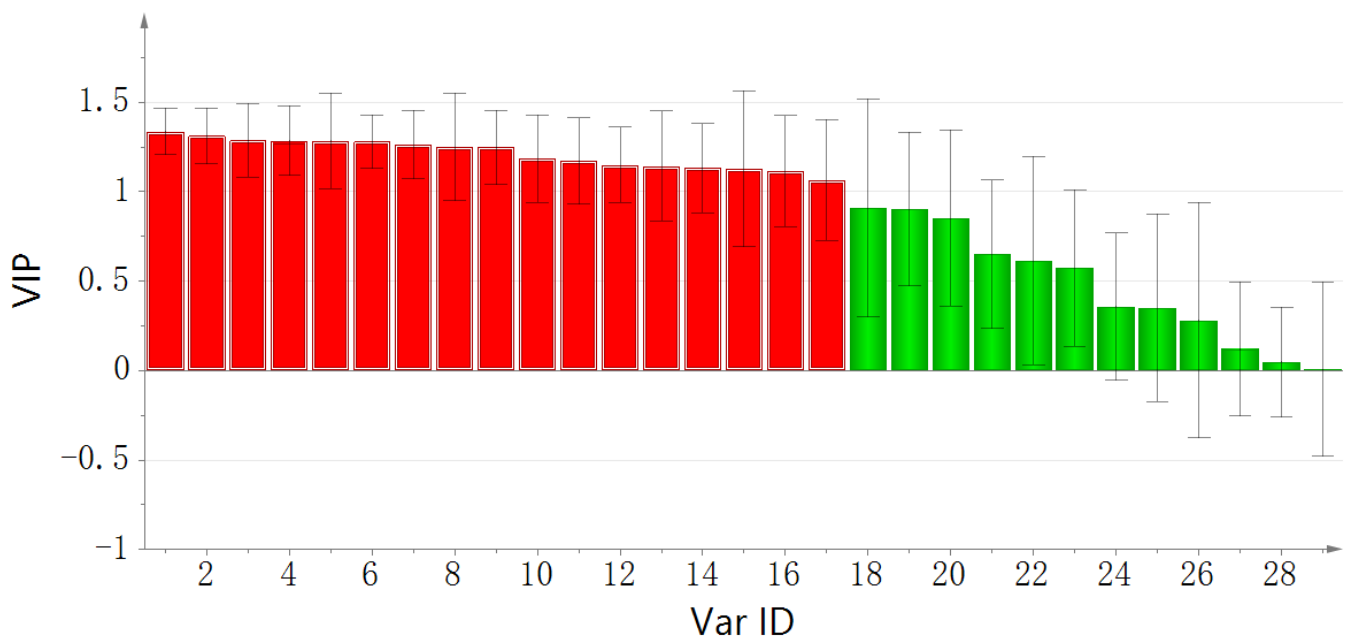


Figure 5. VIP plot of the OPLS-DA model. red indicated VIP value > 1, green indicated VIP value < 1.

3.4. Gray Correlation Analysis

The COX-2 inhibitory efficacy of nine batches of both raw and salt-processed *A. bidentata* samples was evaluated, with the findings presented in Table 5. Inhibition rates for raw *A. bidentata* spanned 58.6% to 73.5%, while those for salt-processed samples ranged from 79.5% to 88%. This implies that *A. bidentata* is strongly associated with COX-2 inhibition and has stronger osteoarthritis therapeutic activity. Correlation coefficients quantifying the relationship between individual compounds and COX-2 inhibition rates are detailed in Table 6. Eight compounds, including sanleng acid, stachysterone D, dihydroactinidiolide, *N-cis*-feruloyl-3-methoxytyramine, *N-trans*-feruloyltyramine, 9,12,13-trihydroxy-10-octadecenoic acid, azelaic acid, and dehydroecdysone, demonstrated a strong positive correlation with COX-2 inhibition. The data indicate a strong correlation between the components and the salt-processed *A. bidentata* in treating osteoarthritis. It is suggested that salt baking significantly contributes to the biological activity of *A. bidentata*. This finding also suggests that the therapeutic effects of salt-processed *A. bidentata* on osteoarthritis may be due to the combined action of multiple compounds.

Table 5. COX-2 inhibitory rate for nine batches of raw and salt-processed *Achyranthes bidentata*.

No.	Inhibitory Rate (%)	No.	Inhibitory Rate (%)
S1	68.5	Y1	81.1
S2	70.4	Y2	81.5
S3	73.5	Y3	79.5
S4	64.7	Y4	89.0
S5	65.6	Y5	81.7
S6	67.5	Y6	82.7
S7	70.2	Y7	82.1
S8	60.2	Y8	88.3
S9	58.6	Y9	83.4

Table 6. Correlation coefficient of compounds from raw and salt-processed *Achyranthes bidentata*.

No.	Compounds	Correlation Coefficient r
1	Maleic acid	0.7450
2	Unknown	0.7574
3	Fumaric acid	0.7326
4	Indolylactic acid	0.8394
5	Methylflavone	0.8060
6	Polypodine B	0.8358
7	Methoxytyrosine	0.7346
8	Ecdysterone	0.8378
9	25R-inokosterone	0.7544
10	25S-inokosterone	0.8381
11	Dehydroecdysone	0.8506
12	Deoxykaladasterone	0.7291
13	Kaladasterone	0.7156
14	Dacryhainansterone	0.7267
15	Azelaic acid	0.8925
16	Liquiritin apioside	0.7818
17	<i>N-cis</i> -feruloyl-3-methoxytyramine	0.9175
18	<i>N-trans</i> -feruloyltyramine	0.9118
19	Feruloylmethoxytyramine	0.8186
20	Unknown	0.6732
21	Dihydroactinidiolide	0.9186
22	Stachysterone D	0.9291
23	Corchorifatty acid F	0.7514
24	9,12,13-Trihydroxy-10,15-octadecadienoic acid	0.8251
25	9,12,13-Trihydroxy-10-octadecenoic acid	0.9107
26	9,10,13-triHOME	0.7601
27	Pinellic acid	0.6485
28	Sanleng acid	0.9981
29	Unknown	0.7320

3.5. COX-2 Inhibitory Assay

The COX-2 inhibitory effects of sanleng acid, stachysterone D, dihydroactinidiolide, *N-cis*-feruloyl-3-methoxytyramine, *N-trans*-feruloyltyramine, 9,12,13-trihydroxy-10-octadecenoic acid, azelaic acid, and dehydroecdysone were evaluated. These compounds are the aforementioned substances that have a strong positive correlation with the rate of COX-2 inhibition. As shown in Figure 6, the positive control celecoxib showed an IC₅₀ (half maximal inhibitory concentration) value of 25.64 nM, which is in agreement with the literature [39]. Sanleng acid, 9,12,13-trihydroxy-10-octadecenoic acid, and azelaic acid exhibited COX-2 inhibitory activity with IC₅₀ values of 40.74 μM, 93.28 μM, and 86.36 μM, respectively. Stachysterone D and dehydroecdysone showed similar COX-2 inhibitory effects with IC₅₀ values of 63.57 μM and 63.92 μM, respectively. Dihydroactinidiolide had an IC₅₀ value of 70.66 μM. *N-cis*-feruloyl-3-methoxytyramine and *N-trans*-feruloyltyramine displayed IC₅₀ values of 120.7 and 121.9 μM, respectively. However, the correlation strength between these compounds and the rate of COX-2 inhibition is not directly related to the corresponding compounds' IC₅₀. Of note, only the COX-2 inhibitory effect of *N-trans*-feruloyltyramine was reported in the literature [40], while the COX-2 inhibitory effect of seven other compounds, including sanleng acid, stachysterone D, dihydroactinidiolide, *N-cis*-feruloyl-3-methoxytyramine, 9,12,13-trihydroxy-10-octadecenoic acid, azelaic acid, and dehydroecdysone, was reported for the first time. The above eight compounds can be used as quality markers to focus on during the quality control of salt-processed *A. bidentata* for the treatment of osteoarthritis. Future studies will further consider the specific mechanisms of these compounds that are strongly associated with anti-COX-2 inhibition in osteoarthritis therapy.

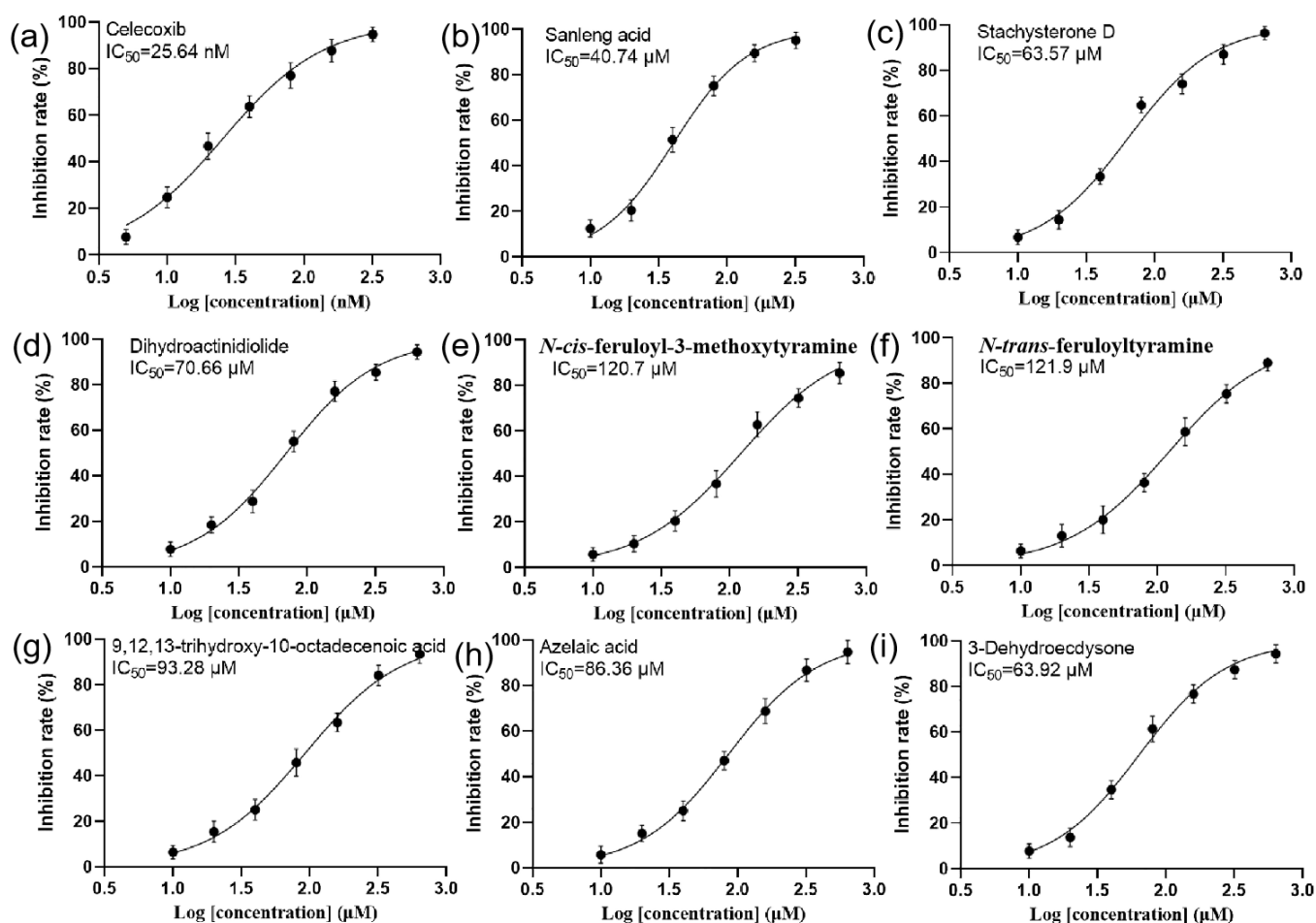


Figure 6. IC₅₀ curves of celecoxib and other compounds. (a) celecoxib, (b) sanleng acid, (c) stachysterone, (d) dihydroactinidiolide, (e) *N-cis*-feruloyl-3-methoxytyramine, (f) *N-trans*-feruloyltyramine, (g) 9, 12, 13-trihydroxy-10-octadecenoic acid, (h) azelaic acid, and (i) dehydroecdysone.

4. Conclusions

A QbD-guided approach was successfully used to optimize the salt-processing parameters of *A. bidentata*. HPLC-Q-TOF-MS analysis combined with orthogonal partial least squares discriminant analysis facilitated the identification of the differential markers between raw and salt-processed *A. bidentata*. Notably, the COX-2 inhibitory effects of seven compounds were identified for the first time, which enhanced our understanding of the anti-inflammatory effects of salt-processed *A. bidentata*. In the future, these compounds can be considered critical product attributes of salt-processed *A. bidentata*.

Supplementary Materials: The following supporting information can be downloaded at: <https://www.mdpi.com/article/10.3390/pr12030434/s1>. Figure S1. Chemical structures of the identified compounds.

Author Contributions: Conceptualization, Y.T. and G.S.; methodology, J.Z. and L.S.; software, J.Z. and L.S.; writing—original draft preparation, J.Z. and L.S.; writing—review and editing, Y.T. and G.S.; supervision, Y.T. and G.S.; and funding acquisition, Y.T. and G.S. All authors have read and agreed to the published version of the manuscript.

Funding: This research was funded by the Hangzhou Municipal Bureau of Science and Technology, grant number 20220919Y164, and the Zhejiang Provincial Natural Science Foundation, grant number LY21H280008.

Data Availability Statement: Data are contained within the article.

Acknowledgments: The authors would like to thank the anonymous reviewers for their invaluable suggestions that helped improve the manuscript.

Conflicts of Interest: The authors declare no conflicts of interest.

References

1. Huang, P.; Tan, S.; Zhang, Y.X.; Li, J.S.; Chai, C.; Li, J.J.; Cai, B.C. The effects of wine-processing on ascending and descending: The distribution of flavonoids in rat tissues after oral administration of crude and wine-processed *Radix scutellariae*. *J. Ethnopharmacol.* **2014**, *155*, 649–664. [[CrossRef](#)]
2. Tao, Y.; Du, Y.; Li, W.; Cai, B.; Di, L.; Shi, L.; Hu, L. Integrating UHPLC-MS/MS quantification and DAS analysis to investigate the effects of wine-processing on the tissue distributions of bioactive constituents of herbs in rats: Exemplarily shown for *Dipsacus asper*. *J. Chromatogr. B* **2017**, *1055–1056*, 135–143. [[CrossRef](#)]
3. Zhu, T.; Liu, X.; Wang, X.; Cao, G.; Qin, K.; Pei, K.; Zhu, H.; Cai, H.; Niu, M.; Cai, B. Profiling and analysis of multiple compounds in rhubarb decoction after processing by wine steaming using UHPLC-Q-TOF-MS coupled with multiple statistical strategies. *J. Sep. Sci.* **2016**, *39*, 3081–3090. [[CrossRef](#)] [[PubMed](#)]
4. Li, W.; Ren, C.; Fei, C.; Wang, Y.; Xue, Q.; Li, L.; Yin, F.; Li, W. Analysis of the chemical composition changes of *Gardeniae Fructus* before and after processing based on ultra-high-performance liquid chromatography quadrupole time-of-flight mass spectrometry. *J. Sep. Sci.* **2021**, *44*, 981–991. [[CrossRef](#)] [[PubMed](#)]
5. Qin, K.; Wang, B.; Li, W.; Cai, H.; Chen, D.; Liu, X.; Yin, F.; Cai, B. Quality assessment of raw and processed *Arctium lappa* L. through multicomponent quantification, chromatographic fingerprint, and related chemometric analysis. *J. Sep. Sci.* **2015**, *38*, 1491–1498. [[CrossRef](#)] [[PubMed](#)]
6. He, X.; Wang, X.; Fang, J.; Chang, Y.; Ning, N.; Guo, H.; Huang, L.; Huang, X. The genus *Achyranthes*: A review on traditional uses, phytochemistry, and pharmacological activities. *J. Ethnopharmacol.* **2017**, *203*, 260–278. [[CrossRef](#)] [[PubMed](#)]
7. Li, Z.; Ma, D.; Peng, L.; Li, Y.; Liao, Z.; Yu, T. Compatibility of *Achyranthes bidentata* components in reducing inflammatory response through Arachidonic acid pathway for treatment of Osteoarthritis. *Bioengineered* **2022**, *13*, 1746–1757. [[CrossRef](#)] [[PubMed](#)]
8. Gawande, D.Y.; Goel, R.K. Pharmacological validation of in-silico guided novel nootropic potential of *Achyranthes aspera* L. *J. Ethnopharmacol.* **2015**, *175*, 324–334. [[CrossRef](#)] [[PubMed](#)]
9. Ishtiaq, A.; Muhammad, I.; Ullah, B.; Muhammad, N.; Muhammad, Z.; Ali, N. Pharmacognostic and hypoglycemic studies of *Achyranthus aspera* L. *J. Pharmacognosy Phytother.* **2013**, *5*, 127–131. [[CrossRef](#)]
10. Pan, R.; Hu, W.; Pan, J.; Huang, L.; Luan, C.; Shen, H. *Achyranthes bidentata* polypeptides prevent apoptosis by inhibiting the glutamate current in cultured hippocampal neurons. *Neural Regen. Res.* **2020**, *15*, 1086–1093.
11. Nazir, A.; Saleem, M.A.; Nazir, F.; Hussain, T.; Faizan, M.Q.; Usman, M. Comparison of UV Protection Properties of Cotton Fabrics Treated with Aqueous and Methanolic Extracts of *Achyranthes aspera* and *Alhagi maurorum* Plants. *Photochem. Photobiol.* **2016**, *92*, 343–347. [[CrossRef](#)]
12. Gawande, D.Y.; Druzhilovsky, D.; Gupta, R.C.; Poroikov, V.; Goel, R.K. Anticonvulsant activity and acute neurotoxic profile of *Achyranthes aspera* Linn. *J. Ethnopharmacol.* **2017**, *202*, 97–102. [[CrossRef](#)]
13. Zhang, S.; Zhang, Q.; Zhang, D.; Wang, C.; Yan, C. Anti-osteoporosis activity of a novel *Achyranthes bidentata* polysaccharide via stimulating bone formation. *Carbohydr. Polym.* **2018**, *184*, 288–298. [[CrossRef](#)]
14. Lee, T.G.; Hyun, S.W.; Jo, K.; Park, B.; Lee, I.S.; Song, S.J.; Kim, C.S. *Achyranthis radix* Extract Improves Urban Particulate Matter-Induced Dry Eye Disease. *Int. J. Environ. Res. Public Health* **2019**, *16*, 3229. [[CrossRef](#)]
15. Wang, S.; Zeng, M.; Li, B.; Kan, Y.; Zhang, B.; Zheng, X.; Feng, W. Raw and salt-processed *Achyranthes bidentata* attenuate LPS-induced acute kidney injury by inhibiting ROS and apoptosis via an estrogen-like pathway. *Biomed. Pharmacother.* **2020**, *129*, 110403. [[CrossRef](#)]
16. Nunavath, R.S.; Singh, M.T.; Jain, A.; Chakma, M.; Arivuselvam, R.; Azeze, M. Quality by Design in Pharmaceuticals: A Review of its Impact on Regulatory Compliance and Product Quality. *Drug Res.* **2024**, *74*, 18–23.
17. Abramson, S.B. The role of COX-2 produced by cartilage in arthritis. *Osteoarthr. Cartil.* **1999**, *7*, 380–381. [[CrossRef](#)] [[PubMed](#)]
18. El-Miligy MM, M.; Al-Kubeisi, A.K.; El-Zemity, S.R.; Nassra, R.A.; Abu-Serie, M.M.; Hazzaa, A.A. Discovery of small molecule acting as multitarget inhibitor of colorectal cancer by simultaneous blocking of the key COX-2, 5-LOX and PIM-1 kinase enzymes. *Bioorg. Chem.* **2021**, *115*, 105171. [[CrossRef](#)] [[PubMed](#)]
19. Lv, Y.; Wu, H.; Hong, Z.; Wei, F.; Zhao, M.; Tang, R.; Li, Y.; Ge, W.; Li, C.; Du, W. Exploring active ingredients of anti-osteoarthritis in raw and wine-processed *Dipsaci Radix* based on spectrum-effect relationship combined with chemometrics. *J. Ethnopharmacol.* **2023**, *309*, 116281. [[CrossRef](#)] [[PubMed](#)]
20. Li, S.; Sun, Y.; Gao, Y.; Yu, X.; Zhao, C.; Song, X.; Han, F.; Yu, J. Spectrum-effect relationship analysis based on HPLC-FT-ICR-MS and multivariate statistical analysis to reveal the pharmacodynamic substances of Ling-Gui-Zhu-Gan decoction on Alzheimer’s disease. *J. Pharm. Biomed. Anal.* **2024**, *237*, 115765. [[CrossRef](#)] [[PubMed](#)]
21. Alam, P.; Siddiqui, N.A.; Rehman, M.T.; Hussain, A.; Akhtar, A.; Mir, S.R.; Alajmi, M.F. Box–Behnken Design (BBD)-Based Optimization of Microwave-Assisted Extraction of Parthenolide from the Stems of *Tarconanthus camphoratus* and Cytotoxic Analysis. *Molecules* **2021**, *26*, 1876. [[CrossRef](#)] [[PubMed](#)]

22. Wen, S.; Tu, X.; Zang, Q.; Zhu, Y.; Li, L.; Zhang, R.; Abliz, Z. Liquid chromatography-mass spectrometry-based metabolomics and fluxomics reveals the metabolic alterations in glioma U87MG multicellular tumor spheroids versus two-dimensional cell cultures. *Rapid Commun. Mass Spectrom.* **2024**, *38*, e9670. [[CrossRef](#)]
23. Sun, J.; Song, Y.; Sun, H.; Liu, W.; Zhang, Y.; Zheng, J.; Zhang, Q.; Zhao, Y.; Xiao, W.; Tu, P.; et al. Characterization and quantitative analysis of phenolic derivatives in Longxuetongluo Capsule by HPLC-DAD-IT-TOF-MS. *J. Pharm. Biomed. Anal.* **2017**, *145*, 462–472. [[CrossRef](#)]
24. Yao, C.; Wang, Y.; Qu, H.; Li, J.; Hou, J.; Chen, X.; Zhang, J.; Wei, W.; Bi, Q.; Guo, D.A. Comparative identification of phytoecdysteroids in *Achyranthes bidentata* Blume and its three analogous species and application in differentiation between processing products from different species. *J. Pharm. Biomed. Anal.* **2023**, *227*, 115187. [[CrossRef](#)]
25. Zhang, L.; Yang, J.Q.; Luo, Y.; Shang, J.C.; Jiang, X.H. Simultaneous determination of eleven compounds related to metabolism of bioamines in rat cortex and hippocampus by HPLC-ECD with boron-doped diamond working electrode. *J. Pharm. Biomed. Anal.* **2016**, *118*, 41–51. [[CrossRef](#)]
26. Yadav, A.; Yadav, S.; Dabur, R. Higher plants exert interspecific effects on the phytoecdysteroids contents in *Tinospora cordifolia*. *Chem. Bio. Lett.* **2022**, *9*, 312.
27. Bourne, P.C.; Whiting, P.; Dhadialla, T.S.; Hormann, R.E.; Girault, J.P.; Harmatha, J.; Lafont, R.; Dinan, L. Ecdysteroid 7,9(11)-dien-6-ones as potential photoaffinity labels for ecdysteroid binding proteins. *J. Insect Sci.* **2002**, *2*, 11. [[CrossRef](#)] [[PubMed](#)]
28. Yang, L.; Jiang, H.; Wang, Q.H.; Yang, B.Y.; Kuang, H.X. A new feruloyl tyramine glycoside from the roots of *Achyranthes bidentata*. *Chin. J. Nat. Med.* **2012**, *10*, 16–19. [[CrossRef](#)]
29. Souza, L.; Oliveira, J.; Fernandes AD, S.; Macedo, A.F.; Araujo-Lima, C.F.; Felzenszwalb, I. UHPLC-MS metabolomic profile and in silico pharmacokinetic approach of *Kalanchoe daigremontiana* Raym.-Hamet & H. Perrier aqueous extracts. *J. Pharm. Biomed. Anal.* **2024**, *238*, 115827.
30. Hamberg, M.; Olsson, U. Efficient and specific conversion of 9-lipoxygenase hydroperoxides in the beetroot. Formation of pinellic acid. *Lipids* **2011**, *46*, 873–878. [[CrossRef](#)]
31. Fuchs, D.; Tang, X.; Johnsson, A.K.; Dahlén, S.E.; Hamberg, M.; Wheelock, C.E. Eosinophils synthesize trihydroxyoctadecenoic acids (TriHOMEs) via a 15-lipoxygenase dependent process. *Biochim. Et Biophys. Acta (BBA)-Mol. Cell Biol. Lipids* **2020**, *1865*, 158611. [[CrossRef](#)]
32. Khan, R.S.; Senthil, M.; Rao, P.C.; Basha, A.; Alvala, M.; Tummuri, D.; Masubuti, H.; Fujimoto, Y.; Begum, A.S. Cytotoxic constituents of *Abutilon indicum* leaves against U87MG human glioblastoma cells. *Nat. Prod. Res.* **2015**, *29*, 1069–1073. [[CrossRef](#)]
33. Mei, Y.; Zhang, X.; Hu, Y.; Tong, X.; Liu, W.; Chen, X.; Cao, L.; Wang, Z.; Xiao, W. Screening and characterization of xenobiotics in rat bio-samples after oral administration of Shen-Wu-Yi-Shen tablet using UPLC-Q-TOF-MS/MS combined with a targeted and non-targeted strategy. *J. Pharm. Biomed. Anal.* **2023**, *227*, 115286. [[CrossRef](#)]
34. Zhou, W.; Wang, P.G. Simultaneous determination of multi-class active pharmaceutical ingredients by UHPLC-HRMS. *J. Pharm. Biomed. Anal.* **2021**, *202*, 114160. [[CrossRef](#)]
35. Aly, S.H.; Elissawy, A.M.; Mahmoud, A.M.A.; El-Tokhy, F.S.; Mageed, S.S.A.; Almahli, H.; Al-Rashood, S.T.; Binjubair, F.A.; Hassab, M.A.E.; Eldehna, W.M.; et al. Synergistic Effect of *Sophora japonica* and *Glycyrrhiza glabra* Flavonoid-Rich Fractions on Wound Healing: In Vivo and Molecular Docking Studies. *Molecules* **2023**, *28*, 2294. [[CrossRef](#)] [[PubMed](#)]
36. Pan, L.; Li, L.; Xu, L.; Zhang, J.; Li, J.; Gao, M.; Yu, J.; Jin, L.; Lei, D. UHPLC-QTOF-MS/MS based characterization of anti-tumor constituents in *Ceratocarpus arenarius* L. and identification of EGFR-TK inhibitors by virtual screening. *Nat. Prod. Res.* **2022**, *36*, 6111–6115. [[CrossRef](#)] [[PubMed](#)]
37. Chang, Q.; Lan, L.; Gong, D.; Guo, Y.; Sun, G. Evaluation of quality consistency of herbal preparations using five-wavelength fusion HPLC fingerprint combined with ATR-FT-IR spectral quantized fingerprint: *Belamcandae rhizoma* antiviral injection as an example. *J. Pharm. Biomed. Anal.* **2022**, *214*, 114733. [[CrossRef](#)] [[PubMed](#)]
38. Yi-meng, Y.; Ke-xin, Y.; Yu-sheng, L.; Ge, C.; Han-wen, T.; Zhongying, L.; Zhiqiang, L.; Fengrui, S.; Zifeng, P. Characterization of Components in Huangying Kechuan Syrup by Ultra-high Liquid Chromatography Tandem Quadrupole-time-of-flight Mass Spectrometry. *Chin. J. App. Chem.* **2021**, *38*, 276.
39. Fadaly, W.A.A.; Nemr, M.T.M.; Zidan, T.H.; Mohamed, F.E.A.; Abdelhakeem, M.M.; Abu Jayab, N.N.; Omar, H.A.; Abdellatif, K.R.A. New 1,2,3-triazole/1,2,4-triazole hybrids linked to oxime moiety as nitric oxide donor selective COX-2, aromatase, B-RAF(V600E) and EGFR inhibitors celecoxib analogs: Design, synthesis, anti-inflammatory/anti-proliferative activities, apoptosis and molecular modeling study. *J. Enzym. Inhib. Med. Chem.* **2023**, *38*, 2290461.
40. Jiang, Y.; Yu, L.; Wang, M.H. N-trans-feruloyltyramine inhibits LPS-induced NO and PGE2 production in RAW 264.7 macrophages: Involvement of AP-1 and MAP kinase signalling pathways. *Chem. Biol. Interact.* **2015**, *235*, 56–62. [[CrossRef](#)] [[PubMed](#)]

Disclaimer/Publisher's Note: The statements, opinions and data contained in all publications are solely those of the individual author(s) and contributor(s) and not of MDPI and/or the editor(s). MDPI and/or the editor(s) disclaim responsibility for any injury to people or property resulting from any ideas, methods, instructions or products referred to in the content.